Design, fabrication and characterization of subwavelength computer-generated holograms for spot array generation

Uriel Levy, Chia-Ho Tsai, Hyo-Chang Kim and Yeshaiahu Fainman

Dept. of Electrical and Computer Engineering, University of California, San Diego, 9500 Gilman Drive, La Jolla CA, 92093-0407. email: ulevy@ece.ucsd.edu
ulevy@ece.ucsd.edu

Abstract: We report the analysis, design, fabrication and experimental characterization of novel subwavelength computer-generated holograms that produce uniform symmetric spot array. We distinguish between a polarization-sensitive and polarization-insensitive far-field reconstruction and show that a linearly polarized incident illumination is required in the former case in order to generate a symmetric reconstruction. The polarization-insensitive case generates a symmetric response independent of the illumination polarization. We show that this response is equivalent to that of a scalar-based computer-generated hologram but with an additional, independent, term that describes the undiffracted zeroth order. These findings simplify the design and optimization of form birefringent computer-generated holograms (F-BCGH) significantly. We present experimental results that verify our analysis and highlight the advantage of these novel elements over scalar-designed elements.

OCIS codes: (260.5430) Polarization; (050.1970) Diffractive optics; (999.9999) Subwavelength gratings

References and Links

1. I. Richter, P. C. Sun, F. Xu and Y. Fainman, "Design considerations of form birefringent microstructures," Appl. Opt. **34,** 2421-2429 (1995).
2. F. Xu, R. Tyan, P. C. Sun, C. Cheng, A. Scherer and Y. Fainman, "Fabrication, modeling, and characterization of form-birefringent nanostructures," Opt. Lett. **20,** 2457-2459, (1995).
3. C. Gu and P. Yeh, "Form birefringence dispersion in periodic layered media," Opt. Lett. **21,** 504-506 (1996).
4. G. Nordin and P. Deguzman, "Broadband form birefringent quarter-wave plate for the mid-infrared wavelength region," Opt. Express **5,** 163-168 (1999).
5. U. Levy and Y. Fainman, "Dispersion properties of inhomogeneous nanostructures," J. Opt. Soc. Am. A. **21,** 881-889 (2004).
6. Z. Bomzon, G. Biener, V. Kleiner and E. Hasman, "Radially and azimuthally polarized beams generated by space-variant dielectric subwavelength gratings," Opt. Lett. **27,** 285-287 (2002).
7. U. Levy, C. H. Tsai, L. Pang and Y. Fainman, "Engineering space-variant inhomogeneous media for polarization control," Opt. Lett. **29,** (2004).
8. Z. Bomzon, G. Biener, V. Kleiner, and E. Hasman, "Space-variant Pancharatnam-Berry phase optical elements with computer-generated subwavelength gratins," Opt. Lett. **27,** 1141-1143 (2002).
9. F. Xu, R. Tyan, P. C. Sun, Y. Fainman, C. Cheng and A. Scherer, "Form-birefringent computer-generated holograms," Opt. Lett. **21,** 1513-1515 (1996).
10. F. T. Chen and H. G. Craighead, "Diffractive phase elements based on two-dimensional artificial dielectrics," Opt. Lett. **20,** 121-123 (1995).
11. P. Lalanne, S. Astilean, P. Chavel, E. Cambril, H. Launois, "Blazed binary subwavelength gratings with efficiencies larger than those of conventional echelette gratings," Opt. Lett. **23,** 1081-1083 (1998).
12. J. N. Mait, A. Scherer, O. Dial, D. W. Prather and X. Gao, "Diffractive lens fabricated with binary features less than 60nm," Opt. Lett. **25,** 381-383 (2000).
13. F. Gori, "Measuring Stokes parameters by means of polarization gratings," Opt. Lett. **24,** 584-586 (1999).
14. G. Biener, A. Niv, V. Kleiner, E. Hasman, "Near-field Fourier transform polarimetry by use of a discrete space-variant subwavelength grating," J. Opt. Soc. Am. A. **20,** 1940-1948 (2003).

#5172 - $15.00 US Received 1 September 2004; revised 18 October 2004; accepted 19 October 2004

15. J. Tervo and J. Turunen, "Paraxial-Domain diffractive elements with 100% efficiency based on polarization gratings," Opt. Lett. **25,** 785-786 (2000).
16. M. Honkanen, V. Kettunen, J. Tervo, and J. Turunen, "Fourier array illuminators with 100% efficiency: analytical Jones-matrix construction," J. Mod. Opt. **47,** 2351-2359 (2000).
17. J. Tervo, V. Kettunen, M. Honkanen and J. Turunen, "Design of space-variant diffractive polarization elements," J. Opt. Soc. Am. A, **20,** 282-289 (2003).
18. S. M. Rytov, "Electromagnetic properties of a finely stratified medium," Sov. Phys. JETP, 2, 466-475, (1956).
19. M. Born and E. Wolf, Principles of Optics, (Cambridge university press 1980), Chap. 14.
20. U. Levy, E. Marom and D. Mendlovic, "Thin element approximation for the analysis of blazed gratings: simplified model and validity limits," Opt. Commun. **229,** 11-21 (2004)
21. S. Kirpatrick, C. D. Gellat, Jr., M. P. Vecchi, "Optimization by simulated annealing," Science, **220,** 671-680 (1983).
22. O. Bryngdahl and F. Wyrowski, "Digital holography – computer-generated holograms," in *Progress in Optics*, E. Wolf, ed. (North-Holland, Amsterdam, 1990), Vol 28, Chap. 1.
23. U. Krackhardt, J. N. Mait, and N. Streibl, "Upper bound on the diffraction efficiency of phase-only fan-out elements," Appl. Opt. **31**, 27-37 (1992).
24. M. G. Moharam, T. K. Gaylord, "Diffraction analysis of dielectric surface-relief gratings," J. Opt. Soc. Am. **72,** 1385 (1982).

1. Introduction

Subwavelength form-birefringent structures can be engineered to artificially create unique anisotropic [1, 2] and dispersive [3-5] properties. The subwavelength grating lines can be distributed within the device aperture both continuously, realizing polarization transformers [6, 7] and polarization beam splitters [8], and discretely using cell-encoded approach, realizing polarization selective elements [9], blazed gratings [10, 11], lenses [12], polarization analyzers [13, 14] as well as array generators [15-17]. In general, these devices utilize optimization of the two independent degrees of freedom, i.e., the orientation of the form-birefringent grating and the amount of birefringence, to control the complex amplitude of the two orthogonally polarized optical field components. In this manuscript we discuss a specific class of form-birefringent computer-generated holograms (F-BCGH) producing symmetric far-field intensity reconstruction for linearly polarized incident fields. Generally, an overall symmetric intensity pattern in the far-field is obtained by the superposition of intensities generated by the two orthogonal circular polarization states, where these intensities are either symmetric or asymmetric. With several simplifying assumptions, we show that for the superposition of symmetric intensity patterns, the overall far-field intensity distribution is polarization insensitive and equivalent to that of the scalar computer-generated hologram (besides the additional freedom to control the zero order independently), whereas for the case of superposition of asymmetric intensity patterns, a linear incident polarization is required in order to produce the desired symmetric overall intensity distribution. We also provide design method that allows limiting the search region of the phase retardation. Our findings are supported by design, fabrication and experimental characterization of a novel F-BCGH elements realizing spot array generation.

The manuscript is organized as follows; we begin with a general theoretical analysis (section 2). Section 3 presents simplified equations for the case of a symmetric array illuminated with linearly polarized light and discusses the relation between phase retardation and central spot intensity. The experimental validation of two design examples (1 by 3 and 1 by 5 array generator elements) is discussed in section 4 followed by conclusions in Section 5.

2. Theoretical analysis

The operation of F-BCGH element is best explained by effective index concept [18] for a grating with a period smaller than the wavelength of optical field in the material. Such structure does not support propagating diffraction orders (besides the zero-th order), but due to difference in polarizability, its overall dielectric properties are similar to these of a negative uniaxial crystal [19]. The effective dielectric constant obtained for TE polarized field (electric

#5172 - $15.00 US Received 1 September 2004; revised 18 October 2004; accepted 19 October 2004

field perpendicular to the subwavelength grating k-vector) is larger than that obtained for TM polarized field (magnetic field perpendicular to the subwavelength grating k-vector), introducing phase retardation between these two polarization components of the incident optical fields. For example, if the depth of the periodic structure is designed to introduce a π phase shift between the TE and TM components, the device will act as a half-wave retardation plate. An incident linearly polarized field will experience rotation of its polarization by twice the angle between the k-vector of the form birefringent structure and the direction of the incident linearly polarized field. By controlling the orientation of the form birefringent structure, we can engineer the amount of rotation in a space-variant manner. The phase retardation is determined by the duty cycle and the etching depth of the subwavelength grating. The F-BCGH approach utilizes a 1-D or 2-D array of cells (see Fig. 1) each containing a subwavelength grating with desired orientation and birefringence.

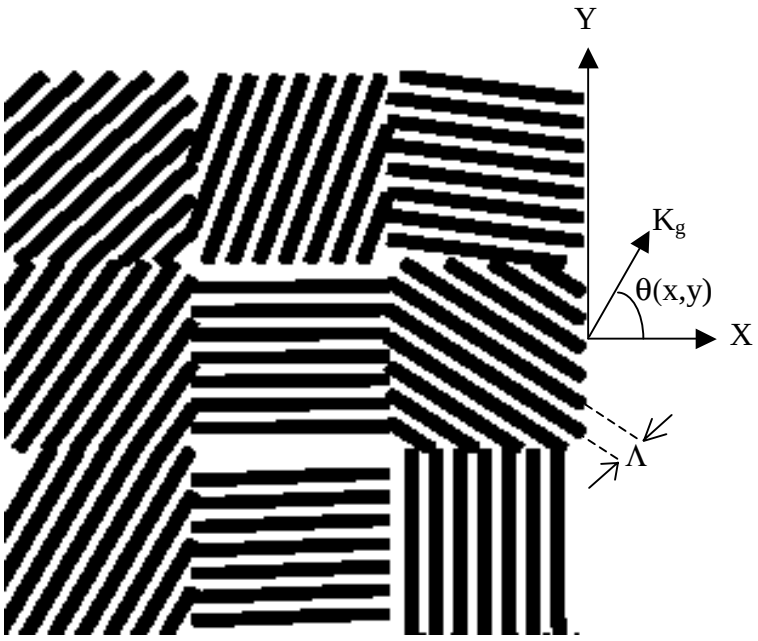

Fig. 1. Schematic diagram of diffractive optical element using subwavelength grating based phase modulation: subwavelngth grating with a period Λ is introduced into each cell with oriantation of the grating θ(x,y).

Next, we analyze the properties of an optical field transmitted through an F-BCGH element made of simple binary profile with a constant duty cycle. Fabrication of such a device will not require complicated calibration and alignment steps. For our analysis we ignore Fresnel reflections from the substrate-air interface since our fabricated devices are usually coated with an anti-reflection (AR) layer on the flat surface. We also assume cell size to be larger then the wavelength of optical fields to allow validity of thin element approximation [20].

Consider a circularly polarized incident plane wave transmitted through the F-BCGH element located at $z = 0$, with x, y being the transverse coordinates. The transmitted optical field is given by:

$$\bar{E}_T\left(x, y, z = 0^+\right) = \bar{\bar{R}}\left(x, y\right)^{-1} \bar{\bar{G}}\bar{\bar{R}}\left(x, y\right)\bar{V}_{in} \tag{1}$$

#5172 - $15.00 US Received 1 September 2004; revised 18 October 2004; accepted 19 October 2004

where $\bar{\bar{R}}(x,y)=\begin{bmatrix}\cos[\theta(x,y)] & \sin[\theta(x,y)]\\ -\sin[\theta(x,y)] & \cos[\theta(x,y)]\end{bmatrix}$ is the rotation matrix and $\bar{\bar{G}}=\begin{bmatrix}\exp(-i\phi/2) & 0\\ 0 & \exp(i\phi/2)\end{bmatrix}$ is the Jones matrix representing the birefringence generated by the subwavelength grating in each cell (with respect to the rotated coordinate system). ϕ is the phase retardation of the grating (its value depends on the etching depth, the grating profile, and the refractive index of the substrate) and is assumed to be space invariant under the assumption of constant etch depth and constant duty cycle made above. In general, however, the phase retardation (and therefore $\bar{\bar{G}}$) can be space variant. $\theta(x,y)$ is the local rotation angle of the subwavelength grating in each cell. For incident right- and left-hand circularly polarized light described by the corresponding Jones vectors, $\bar{V}_{inR}=\begin{bmatrix}1\\ j\end{bmatrix}$ and $\bar{V}_{inL}=\begin{bmatrix}1\\ -j\end{bmatrix}$ we use Eq. (1) and obtain the transmitted field given by,

$$\bar{E}_{TR}(x,y,z=0^{+})=\cos(\phi/2)\begin{bmatrix}1\\ j\end{bmatrix}-j\sin(\phi/2)\exp[+j2\theta(x,y)]\begin{bmatrix}1\\ -j\end{bmatrix} \tag{2a}$$

and

$$\bar{E}_{TL}(x,y,z=0^{+})=\cos(\phi/2)\begin{bmatrix}1\\ -j\end{bmatrix}-j\sin(\phi/2)\exp[-j2\theta(x,y)]\begin{bmatrix}1\\ j\end{bmatrix} \tag{2b}$$

respectively. Similar result can be found also in Ref [8].

For various applications including spot array generation, far-field intensity distribution is of main concern. In the far-field one obtains,

$$\tilde{\bar{E}}_{R}(x',y')=\int_{-\infty}^{+\infty}\int\bar{E}_{TR}(x,y)\exp[-j2\pi(xx'+yy')]dxdy=$$
$$\cos(\phi/2)\delta_{d}(x',y')\begin{bmatrix}1\\ j\end{bmatrix}-j\sin(\phi/2)\int_{-\infty}^{+\infty}\int\exp[j2\theta(x,y)]\exp[-j2\pi(xx'+yy')]dxdy\begin{bmatrix}1\\ -j\end{bmatrix} \tag{3a}$$

and

$$\tilde{\bar{E}}_{L}(x',y')=\int_{-\infty}^{+\infty}\int\bar{E}_{TL}(x,y)\exp[-j2\pi(xx'+yy')]dxdy=\cos(\phi/2)\delta_{d}(x',y')\begin{bmatrix}1\\ -j\end{bmatrix}-$$
$$j\sin(\phi/2)\int_{-\infty}^{+\infty}\int\exp[-j2\theta(x,y)]\exp[-j2\pi(xx'+yy')]dxdy\begin{bmatrix}1\\ j\end{bmatrix}=\cos(\phi/2)\delta(x',y')\begin{bmatrix}1\\ -j\end{bmatrix} \tag{3b}$$
$$-j\sin(\phi/2)\left\{\int_{-\infty}^{+\infty}\int\exp[j2\theta(x,y)]\exp[-j2\pi(x(-x')+y(-y'))]dxdy\right\}^{*}\begin{bmatrix}1\\ j\end{bmatrix}$$

where ~ and * denote Fourier transform and complex conjugate operations respectively, *x', y'* are the normalized transverse spatial coordinates in the far-field (the constant λz factor was ignored) and $\delta_{d}(x',y')$ is the dirac delta function.

By comparing Eq. (3a) and (3b) it is evident that

#5172 - $15.00 US Received 1 September 2004; revised 18 October 2004; accepted 19 October 2004

$$\left|\tilde{E}_R(x',y')\right| = \left|\tilde{E}_L(-x',-y')\right| \tag{4}$$

This mirror-symmetry property is of major importance, and will be used to analyzed the F-BCGH performances.

It is useful to distinguish between two cases when (A) $\left|\tilde{E}_{R,L}(x',y')\right|$ are asymmetric, i.e. $\left|\tilde{E}_{R,L}(x',y')\right| \neq \left|\tilde{E}_{R,L}(-x',-y')\right|$ and when (B) $\left|\tilde{E}_{R,L}(x',y')\right|$ is symmetric, i.e. $\left|\tilde{E}_{R,L}(x',y')\right| = \left|\tilde{E}_{R,L}(-x',-y')\right|$.

A. Asymmetric field:

In general, the incident field is elliptically polarized,

$$\bar{V}_{in} = \begin{bmatrix} \cos(\chi)\exp(-j\delta/2) \\ \sin(\chi)\exp(+j\delta/2) \end{bmatrix}, \tag{5}$$

where $\tan(\chi)$ denotes the magnitude ratio between the two Cartesian components of the electric field, and δ is the phase difference between these two components. Elliptic polarization state can be described as a linear superposition of the two orthogonal circular polarization states,

$$\bar{V}_{in} = \alpha\begin{bmatrix} 1 \\ j \end{bmatrix} + \beta\begin{bmatrix} 1 \\ -j \end{bmatrix} \tag{6}$$

where α, β are the weighting coefficients given by:

$$2\alpha = \cos(\chi - \delta/2) - j\sin(\chi + \delta/2), \quad 2\beta = \cos(\chi + \delta/2) + j\sin(\chi - \delta/2) \tag{7}$$

and satisfying $|\alpha|^2 + |\beta|^2 = 1$. The overall far-field intensity distribution is obtained by a weighted summation of intensities corresponding to the two orthogonally polarized fields, yielding

$$I(x',y') = |\alpha|^2\left|\tilde{E}_R(x',y')\right|^2 + |\beta|^2\left|\tilde{E}_L(x',y')\right|^2 = |\alpha|^2\left|\tilde{E}_R(x',y')\right|^2 + |\beta|^2\left|\tilde{E}_R(-x',-y')\right|^2, \tag{8}$$

where we used Eq. (4). It is evident that an overall symmetric intensity distribution is achieved only with $|\alpha|^2 = |\beta|^2$. The corresponding values of χ, δ derived from Eq. (7) need to satisfy

$$\cos^2(\chi - \delta/2) - \cos^2(\chi + \delta/2) = 0, \tag{9}$$

yielding

$$\chi = n\pi/2 \text{ or } \delta = m\pi \tag{10}$$

where n, m are integers. Notice that the last equation is a definition of a linearly polarized light. Therefore, for the case where the far-field intensity pattern produced by each of the circular polarization components is a-symmetric, achieving an overall symmetric far-field intensity pattern will be possible only with linearly polarized incident optical field. This result can be understood intuitively by observing the Poincare sphere: each coordinate that is having the same distance from the north and the south pole (corresponding to right and left circular polarization) must be located on the equator plane (which corresponds to the linear

#5172 - $15.00 US Received 1 September 2004; revised 18 October 2004; accepted 19 October 2004

polarization states). Since the overall far-field intensity pattern depends on the incident polarization, we refer to this case as "polarization sensitive beam shaping".

B. Symmetric field: When $\left|\tilde{E}_{R,L}\left(x',y'\right)\right|$ is symmetric, the far-field intensity patterns produced by both of the two circularly polarized terms are identical yielding

$$I_L\left(x',y'\right)=\left|\tilde{E}_L\left(x',y'\right)\right|^2=\left|\tilde{E}_R\left(-x',-y'\right)\right|^2=\left|\tilde{E}_R\left(x',y'\right)\right|^2=I_R\left(x',y'\right) \tag{11}$$

Since an arbitrary incident polarization state can be decomposed onto circular orthogonal basis, the obtained overall far-field intensity pattern is polarization insensitive. We now show that for such case the F-BCGH is equivalent to scalar computer-generated hologram (CGH).

Generally, the field distribution behind a scalar phase only CGH is given by

$$\bar{E}_s\left(x,y,z=0^+\right)=\exp\left[\,j\Phi\left(x,y\right)\right]\,, \tag{12}$$

with $2\theta\left(x,y\right)=\Phi\left(x,y\right)$ and neglecting the first constant cosine term in Eq. (2) (contributing only to the zero order) leading to

$$\bar{E}_{TR}\left(x,y,z=0^+\right)=\bar{E}_s\left(x,y,z=0^+\right)\,, \tag{13a}$$

and to the corresponding far-field

$$\tilde{E}_R\left(x',y'\right)=\tilde{E}_S\left(x',y'\right), \tag{13b}$$

The overall intensity distribution is now

$$I\left(x',y'\right)=\left|\alpha\right|^2\left|\tilde{E}_R\left(x',y'\right)\right|^2+\left|\beta\right|^2\left|\tilde{E}_L\left(x',y'\right)\right|^2=\left|\tilde{E}_R\left(x',y'\right)\right|^2=\left|\tilde{E}_S\left(x',y'\right)\right|^2=I_S\,, \tag{14}$$

where scalar field intensity was defined, $I_S=\left|\tilde{E}_S\left(x',y'\right)\right|^2$.

Equation (14) shows that when $\left|\tilde{E}_R\left(x',y'\right)\right|$ is symmetric our F-BCGH will be equivalent to a scalar element. Nevertheless, even in such a case there is an advantage using the F-BCGH if the central spot is also desired (as in the case of 2N+1 desired spots). This is because of the additional cosine term (see Eq. (2)). The significance of this term will be discussed in the next section. Additional advantage is purely technological – since continuous phase modulation is obtained by the rotation of the binary subwavelength grating lines, there is no longer need for complicated, multi-level fabrication processes.

In summary, when the far-field intensity pattern produced by each of the circularly-polarized components is a-symmetric, will be the only possibility to achieve overall symmetric far-field intensity pattern can be achieved only with linearly polarized incident beam, and the intensity pattern is polarization sensitive. On the other hand, when the intensity pattern produced by each of the circularly polarized components is symmetric, the overall far-field intensity pattern is always symmetric and polarization insensitive, similarly to the scalar case. The practical significance of these conclusions implies that when symmetric intensity pattern is desired there is no longer need to search for an input polarization state during the optimization process – linearly polarized light can always be chosen, significantly reducing computational effort and complexity.

The advantage of our subwavelength CGH over the scalar CGH can be well understood using the example of a desired symmetric array having 2N spots along the x'- axis. This can be achieved with

#5172 - $15.00 US Received 1 September 2004; revised 18 October 2004; accepted 19 October 2004

$$\left|\tilde{E}_R\right|^2 = a\sum_{n=1}^{N}\delta_d\left(x'-n\Delta x'\right)+b\sum_{n=1}^{N}\delta_d\left(x'+n\Delta x'\right), \tag{15}$$

where for simplicity we assume that the far-field distribution is described by a superposition of delta functions. *a* and *b* can be chosen arbitrarily. Using Eq. (4),

$$\left|\tilde{E}_L\right|^2 = b\sum_{n=1}^{N}\delta_d\left(x'-n\Delta x'\right)+a\sum_{n=1}^{N}\delta_d\left(x'+n\Delta x'\right) \tag{16}$$

and the overall symmetric intensity pattern (assuming a linearly polarized incident field) is given by

$$I = \left|\tilde{E}_R\right|^2 + \left|\tilde{E}_L\right|^2 = (a+b)\left[\sum_{1}^{N}\delta\left(x'-\Delta x'\right)+\sum_{1}^{N}\delta\left(x'+\Delta x'\right)\right] \tag{17}$$

As shown, the ratio b/a can be arbitrarily chosen such that the far-field intensity pattern can be optimized with respect to a pre-defined figure of merit. Clearly, this is an important advantage compared with the standard scalar design, which is equivalent to the $b=a$ case. This example can be easily extended to non-uniform spot array by letting the coefficients *a,b* be inside the summation.

3. Design of symmetric array generators

Next we consider the example of a symmetric spot array generation application, and following the above discussion we use linearly polarized incident beam. For reference, we choose the incident polarization to be parallel to the y-axis. Notice that rotating the polarization angle will not change the far-field intensity pattern since it will only add a constant phase term to each of the decomposition coefficients α, β in Eq. (6).

Linearly polarized incident field along the y-axis corresponds to superposition in Eq. (6) with $\alpha=\frac{1}{2j}$, $\beta=-\frac{1}{2\mathrm{j}}$, simplifying Eq. (2),

$$\bar{E}_T\left(x,y,z=0^+\right) = -j\sin(\phi/2)\sin\left[2\theta(x,y)\right]\hat{x}-\left\{\cos(\phi/2)+j\sin(\phi/2)\cos\left[2\theta(x,y)\right]\right\}\hat{y} \tag{18}$$

The obtained transmitted field is a vector described by two orthogonal Cartesian components. The overall far-field intensity pattern is given by an incoherent summation of their Fourier transform, i.e.,

$$I(x',y') = \left|\tilde{E}_x(x',y')\right|^2+\left|\tilde{E}_y(x',y')\right|^2 = \cos^2(\phi/2)\delta_d(x',y')+\sin^2(\phi/2)\times$$
$$\times\left\{\left\{\int_{-\infty}^{\infty}\int\sin\left[2\theta(x,y)\right]\exp\left(j2\pi\left(xx'+yy'\right)\right)dxdy\right\}^2+\left\{\int_{-\infty}^{\infty}\int\cos\left[2\theta(x,y)\right]\exp\left(j2\pi\left(xx'+yy'\right)\right)dxdy\right\}^2\right\} \tag{19}$$

where $\tilde{E}_x(x',y')$ and $\tilde{E}_y(x',y')$ are the Fourier transform components of $\bar{E}_T(x,y)\hat{x}$ and $\bar{E}_T(x,y)\hat{y}$ respectively.

Using Eq. (19) one can now calculates the intensity at the far-field origin (the zeroth diffraction order term),

$$I(x'=0,y'=0) = \cos^2(\phi/2)+\sin^2(\phi/2)\left\{\left\{\int_{-\infty}^{\infty}\int\sin\left[2\theta(x,y)\right]dxdy\right\}^2+\left\{\int_{-\infty}^{\infty}\int\cos\left[2\theta(x,y)\right]\right\}^2\right\} \tag{20}$$

#5172 - $15.00 US Received 1 September 2004; revised 18 October 2004; accepted 19 October 2004

The last equation demonstrates an additional advantage of the F-BCGH device: by modifying the phase retardation ϕ, the intensity of the central spot can be independently controlled, without modifying the relative intensity distribution of the other spots. Obviously, the absolute intensity values will be changed to maintain conservation of energy, as demonstrated by the sine term. This is not always the case for a scalar CGH.
Following Eq. (20), the designed phase retardation needs to satisfy:

$$\cos^2(\phi/2) \le I(0,0) \tag{21}$$

For an example application where the central spot needs to be diminished (as in the case of symmetric array with even number of spots), the phase retardation obeys $\phi = (2n+1)\pi$ where *n* is an integer. To relax the fabrication requirements we usually choose *n=0*. For the typical application where 2N+1 equal intensity spots are desired, the phase retardation is limited by

$$\phi_{\min} = 2\cos^{-1}\left(\frac{1}{\sqrt{2N+1}}\right) \tag{22}$$

As N increases, $\phi_{\min}$ tends towards the asymptotic value of π. By using Eq. (22) the search region for the phase retardation, ϕ is restricted, significantly reducing the computational effort during the optimization process.

4. Experimental validation of the spot array generation

For experimental validation of our novel design methodology we chose to investigate 1 by 3 and 1 by 5 array generators. To optimize the rotation angle $\theta(x',y')$ along the F-BCGH element we used a slightly modified version of the simulated annealing optimization procedure [21]. This optimization engine is computation intensive but in comparisong to iterative-Fourier-transform-algorithm (IFTA) [22], provides more freedom in choosing the cost function. Detailed comparison between the two algorithms is beyond the scope of this paper.

For the optimization we set an initial value for ϕ (see Eq. (22)), an initial pixilated random profile of $\theta(x,y)$ and an initial temperature T. As an error metric, we used

$$e = \sum_{x',y' \in ROI} \sum \left| \eta I_{desired}(x',y') - I_{obtained}(x',y') \right| \tag{23}$$

where ROI denotes region of interest, η is the desired diffraction efficiency, and $I_{obtained}(x',y')$ is calculated using Eq. (19). An initial error value was calculated using Eq. (23). Next we modified the rotation angle $\theta(x,y)$ for a specific cell and observed the evolution of the error. The new value of $\theta(x,y)$ was accepted only if $E = \exp\left[-(e_{new} - e_{old})/T\right] > P$, where P is a random number (*0<P<1*). e_{new} and e_{old} are the error values before and after applying the modification, respectively. In a case where the modification was accepted, the old error value was replaced by the new one. We repeated the described procedure for all the cells 50 times. This was defined as a single iteration. Next, we reduced the temperature (from trail and error experience we have chosen $T = T_0/\left[3\ln(1+it)\right]$ as a typical cooling rate, where *it* denotes the number of iterations) and a new iteration was carried. Once stabilization occurred (i.e., less than 5 modifications are accepted within a single iteration), the optimization process was completed.

#5172 - $15.00 US Received 1 September 2004; revised 18 October 2004; accepted 19 October 2004

Typically, there is a general trade off between the diffraction efficiency and the uniformity of the obtained reconstruction, such that 100% efficiency with perfect uniformity is not always possible to achieve. For our validation examples we set the uniformity threshold to 0.997 (the uniformity is defined as the ratio between the minimal and the maximal intensity within the array), thereby allowing an intensity variation of about 0.3%. First we set the efficiency value η to 1 and observed the uniformity (which was typically smaller than the threshold value). We then gradually decreased the efficiency parameter to a value that allowed to achieve our stringent uniformity requirement.

Our first example on 1 by 3 array generation with three equal intensity spots uses the subwavelength F-BCGH device parameters that can be calculated analytically [15], yielding 100% diffraction efficiency and perfect uniformity for an element with linear phase function for each of the circular polarization components, obtained by setting $\theta(x) = \pi x / d$, where d determines the deflection angle of the diffracted field. With a linear incident polarization, we will reconstruct 2 symmetric off axis spots in the far-field .By choosing $\phi = 0.608\pi$ (using Eq. (22)), a zeroths diffraction order term with equal intensity will also appear, producing a total of 3 spots. For comparison, we tested our optimization procedure and obtained the same design parameters. Notice that for scalar computer-generated hologram the predicted diffraction efficiency calculated using IFTA is 92.5% (although the upper bound for diffraction efficiency is slightly higher [23]).

For the additional example of 1 by 5 array generation there is no known analytic solution. Using our optimization scheme an efficiency prediction of 96.5% with the corresponding phase retardation value of 0.74π was obtained. In comparison, for a scalar computer-generated hologram the predicted diffraction efficiency calculated using IFTA is 91.9%.

For realization of 1 by 3 and 1 by 5 array generators we employed standard microfabrication procedure by generating lithographic e-beam mask followed by photolithography and chemically assisted ion beam etching (CAIBE) to transfer the structure into a GaAs substrate. First, we prepared the grating structure in a format of a GDSII file that was used for the fabrication of the e-beam mask. The orientation of the grating lines matched the $\theta(x, y)$ data obtained from the design procedure. To ensure that the desired structure is indeed equivalent to a uniaxial crystal, the subwavelength-grating period, Λ was chosen to meet our effective medium assumptions $\Lambda < \lambda / n$, where λ is the optical wavelength and n is the refractive index of the substrate. To ease on the fabrication procedures we chose to test our approach for applications at a longer wavelength of CO_2 laser operating at $\lambda = 10.6\ \mu$m. Since we used a GaAs substrate with refractive index of 3.13 at $\lambda = 10.6\ \mu$m, the grating period need to be smaller than $3.38\ \mu$m. To reduce dispersion effects [5] we used a period of $\Lambda = 2.5\ \mu$m. To avoid overlapping between the neighboring spots, the structure was replicated 4 times along the x-axis. The element was designed to have 32 cells per period, resulting in a total number of 128 cells. We set the cell size to $100\ \mu$m, leading to a total aperture of 12.8 mm along the x-axis and a period of d=320 μm. To generate a rectangular element, the aperture along the y- axis was also set to 12.8 mm.

Once the e-beam mask was fabricated, the pattern was transferred into the photoresist (BPRS100) by high-resolution photolithography using Karl Suss MJB3 contact mask aligner. CAIBE process was used to transfer the pattern into the GaAs substrate that was AR coated on its backside to avoid multiple reflections.

To estimate the etching depth required to achieve the desired value of retardation ϕ, we employed rigorous coupled wave analysis (RCWA) [24]. For a duty cycle of 50%, the required depths are 3.2 and 4.2 micron for achieving retardation of 0.608π and 0.74π respectively. The above calculations assume a rectangular groove profile, leading to undesired Fresnel reflection at the grating-air boundary. To minimize these reflection effects, we tuned our fabrication

#5172 - $15.00 US Received 1 September 2004; revised 18 October 2004; accepted 19 October 2004

process to achieve slightly trapezoidal shape [1]. The etching depth was increased by ~10% to maintain the desired retardation. Figure 2 shows a scanning electron microscope (SEM) image of the fabricated device, having a close match to the fabricated profile.

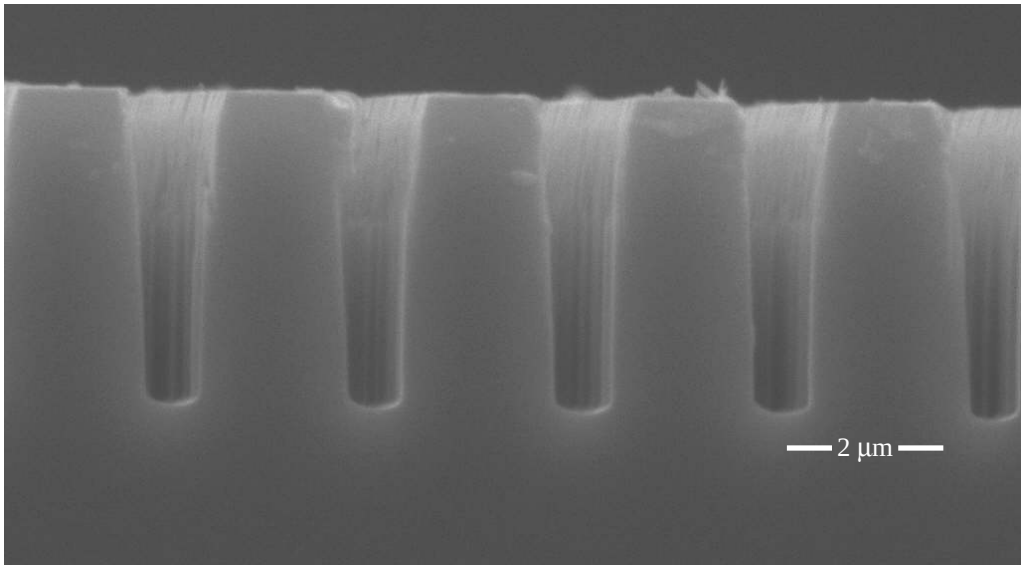

Fig. 2. Typical SEM cross section of the fabricated F-BCGH 1X3 element

Characterization of the fabricated devices was performed using a linearly polarized beam derived from a single mode CO_2 laser source (Synrad 48-1). The F-BCGH element was illuminated with a converging beam producing a Fourier transform plane at a distance $z = 80$ cm from the element. The separation distance between the neighboring reconstructed spots is $L \approx \lambda z / d = 2.65$ mm. The Fourier transform plane was then imaged onto a CCD camera (Indigo Omega) with a demagnification ratio of ~1:5. Fig. 3 shows the images obtained by illuminating the 1 by 3 and the 1 by 5 spot array generator F-BCGH elements, respectively. Corresponding intensity profiles along the horizontal cross sections of Figs. 3 are shown in Fig. 4.

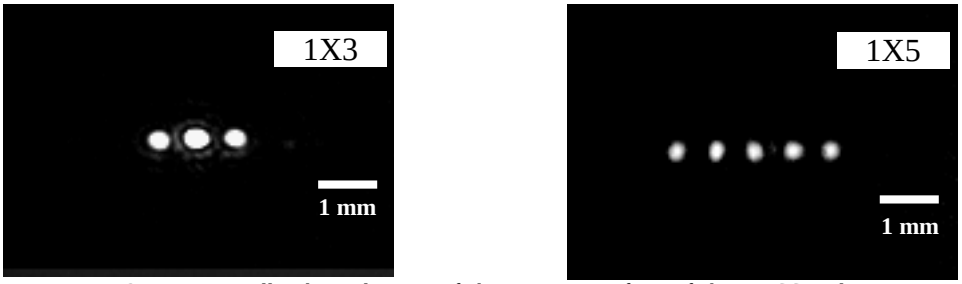

Fig. 3. Experimentally obtained image of the Fourier transform of the F-BCGH element illuminated by a linearly polarized beam.

The horizontal cross section was obtained by subtracting the camera background noise and integrating the data in Fig. 3 along the y- coordinate. Good uniformity (better than 85%) was achieved for both cases. In particular, it should be noted that the central peak (the zeroth diffraction order term) is comparable to the other diffraction orders. Controlling of the central peak is very challenging due to high sensitivity to fabrication inaccuracies. The slight nonuniformity can be explained by small non-uniformity of the photoresist thickness along the

#5172 - $15.00 US Received 1 September 2004; revised 18 October 2004; accepted 19 October 2004

aperture of the F-BCGH. The diffraction efficiency is also high, as evident by the lack of higher diffraction orders. It should be noted, that precise measurement of the diffraction efficiency was not possible due to the thermal background noise in the CCD camera.

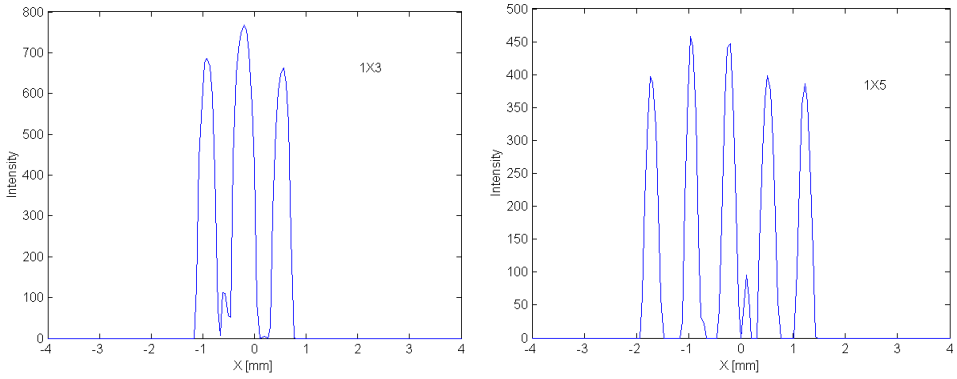

Fig. 4. Cross-section of Fig 3. The cross section was calculated by integrating Fig. 3 along the vertical axis.

5. Conclusions

We used form birefringent computer-generated holograms (F-BCGH) to design, analyze and experimentally demonstrate uniform symmetric spot arrays. These elements are implemented by the fabrication of sub-wavelength binary gratings using standard microfabrication techniques. We made a distinction between polarization sensitive and polarization insensitive far-field intensity reconstruction, showing that in the former case performances exceeding the scalar theory prediction can be obtained and that a linear incident polarization state is required in order to achieve an overall symmetric far-field intensity pattern. In the polarization insensitive case the generated far-field intensity pattern was shown to be equivalent to that produced by a scalar diffractive optical element. Nevertheless, the latter case still offer an advantage compare with scalar diffractive elements by allowing independent control of the zeroth diffraction order term. These findings simplify the design and the optimization of the F-BCGH elements significantly. Numeric simulations and experimental results are provided to support the presented analysis.

Acknowledgments

This work is supported in part by Air Force Office of Scientific Research, the National Science Foundation, the Defense Advanced Research Projects Agency, and the Space and Naval Warfare Systems Command.

#5172 - $15.00 US Received 1 September 2004; revised 18 October 2004; accepted 19 October 2004